ISSN 0016-7029, Geochemistry International, 2023, Vol. 61, No. 9, pp. 948–955. © Pleiades Publishing, Ltd., 2023.
Russian Text © The Author(s), 2023, published in Geokhimiya, 2023, Vol. 68, No. 9, pp. 938–946.

Partitioning and Speciation of Lanthanides in the Magnetite (Hematite)–Hydrothermal Solution System at 450°C and 100 MPa

N. V. Smagunov[a], *, S. V. Lipko[a], **, V. L. Tauson[a], *, O. Yu. Belozerova[a], ****, and D. N. Babkin[a], *******

[a] *A.P. Vinogradov Institute of Geochemistry, Siberian Branch, Russian Academy of Sciences, Irkutsk, 664033 Russia*

**e-mail: nicksm@igc.irk.ru*

***e-mail: slipko@yandex.ru*

****e-mail: vltauson@igc.irk.ru*

*****e-mail: obel@igc.irk.ru*

******e-mail: dimit172@mail.ru*

Received March 15, 2023; revised April 10, 2023; accepted April 16, 2023

Abstract—First results of the experimental study of a hydrothermal multisystem including lanthanides (*Ln*) and Fe oxides (magnetite and hematite) are presented. *Ln* concentrations in solutions and crystals were determined by ICP-MS and LA-ICP-MS, respectively. The *Ln* partition and cocrystallization coefficients obtained are interpreted as the maximum estimates of "true" values corresponding to structurally bound admixture. It is shown that *Ln* (except for Eu) are the compatible elements in hydrothermal magnetite; heavy *Ln* (beginning with Tb) are compatible in hematite. The pronounced tendency of the increase of both coefficients with increasing *Ln* atomic number beginning from Gd–Tb was established. This is of great importance when light to heavy Ln ratio is used as a typochemical guide for localization of ore source. The *Ln*-rich phases in association with magnetite and hematite were obtained. These phases have oxychloride (without Fe) and oxyhydroxide (with Fe) composition and exemplify the simultaneous occurrence of light and heavy *Ln* within a single hydrothermal system due to the co-crystallization of phases selectively accumulating light and heavy lanthanides.

Keywords: experiment, lanthanides, magnetite, hematite, hydrothermal system, partition coefficient, cocrystallization coefficient, speciation

DOI: 10.1134/S0016702923090094

INTRODUCTION

Rare-earth elements (REE), including lanthanide group (*Ln*), are ascribed to strategic metals. They are widely applied in different high-tech fields and are termed as "industrial vitamins" (Chen et al., 2022). The limited REE resources highlight the problems of exploration of their deposits and improvement of mining methods, as well as rational exploitation of host secondary raw material. The solution of these problems requires knowing of REE behavior in heterogeneous systems, their partitioning and solubility constants, characteristics of absorption, and speciation in minerals and chemical compounds.

Magnetite and hematite are frequently present in the REE-bearing iron ore deposits (Tallarico et al., 2005; Harlov et al., 2016), including the largest deposits, for instance, the world-class Bayan-Obo Fe–REE–Nb deposit (Inner Mongolia, China) (Huang et al., 2015). Magnetite and hematite are usually not considered as the main REE carriers (Kulik and Melgunov, 1992; Zamanian and Radmard, 2016), since REE are mainly hosted in calcium minerals–-fluorite, calcite, dolomite, and apatite. In this relation, the REE partition and co-crystallization coefficients in iron oxides practically have not been studied. This is a significant omission given the useful properties of magnetite as an indicator of composition of mineral-forming medium (Smagunov et al., 2021). This work reports the first results of study of multisystem, which includes practically all lanthanides and Fe oxides, magnetite and hematite, under hydrothermal conditions. The values of partition and co-crystallization coefficients were obtained and *Ln*-rich phases associated with these minerals were studied.

EXPERIMENTAL PROCEDURE AND ANALYTICAL METHODS

Experiments were performed using conventional technique of thermogradient hydrothermal synthesis

at 450°C and 100 MPa (1 kbar) coupled with internal sampling of a high-temperature fluid for determination of its composition (Tauson et al., 2018; Smagunov et al., 2021). The experiments were carried out in stainless steel autoclaves ~200 cm^3 in volume designed at the Institute of Crystallography of the Russian Academy of Sciences (Fig. 1). The autoclaves were equipped with titanium (VT-8) passivated containers (inserts) ~50 cm^3 in volume, the upper part of which contains titanium fluid trap. For the first four days, isothermal conditions were maintained to homogenize the system. For subsequent twenty days, a temperature drop of 15°C was applied to the external walls of the autoclave, which corresponds to the actual temperature gradient T of ~0.1 degree/cm for this configuration of experiment.

The experiments were completed with autoclave quenching in cold flowing water with a temperature drop of ~5 degree/s. When inserts were recovered, solution was extracted from trap (solution pH was 8.3–8.4) and the trap was rinsed with aqua regia. Then, it was combined with rinsed waters and analyzed by atomic absorption spectrometry (for Fe) and inductively coupled plasma mass spectrometry (for *Ln*). However, the capture of fluid in trap is not controlled and to certain extent, is an occasional event. For this reason, the amount of captures solution is frequently insufficient and it is required to repeat the experiment.

Ammonium chloride solutions (10%) was used as a mineralizing solution for synthesis of magnetite (runs 1 and 2), while a batch contained all lanthanides, except for promethium. In run 1, 5 g Fe_2O_3 + FeO in 0.8 mol ratio was added with 0.88 wt % of each *Ln* in form of oxide III (IV for Ce). In run 2, 5 g Fe_2O_3 + FeO in 0.5 molar ratio was added with 1.56 wt % of each *Ln* in the same form.

Hematite (runs 3 and 4) was synthesized in run 3 using 5% NH_4Cl solution and batch consisting of 5 g Fe_2O_3 and 0.88 wt % of each *Ln* in form of oxide III (IV for Ce). In run 4, we used 10% NH_4Cl, while batch contained 5 g Fe_2O_3 and 1.56 wt % of each *Ln* in the same form.

The starting materials were prepared from Fe_2O_3 and FeO of analytical grade, NH_4Cl of high purity grade, and lanthanide oxides III and CeO_2 (99.0 to 99.93% of main components) manufactured by different companies.

The *Ln* contents in solutions were determined by ICP-MS on a high-resolution ELEMENT-2 mass-spectrometer (Finnigan MAT, Germany) at the Institute of Geochemistry of the Siberian Branch of the Russian Academy of Sciences. Operation conditions were as follows: generator power of 1200 W, reflected power <4 W, the gas flow (argon) rate of 0.8–0.95, 16 and 0.9–1.2 L/min for transporting, plasma-forming, and auxiliary flows, respectively, the solution supply rate of 0.9 mL/min, Meinhard concentric nebulizer,

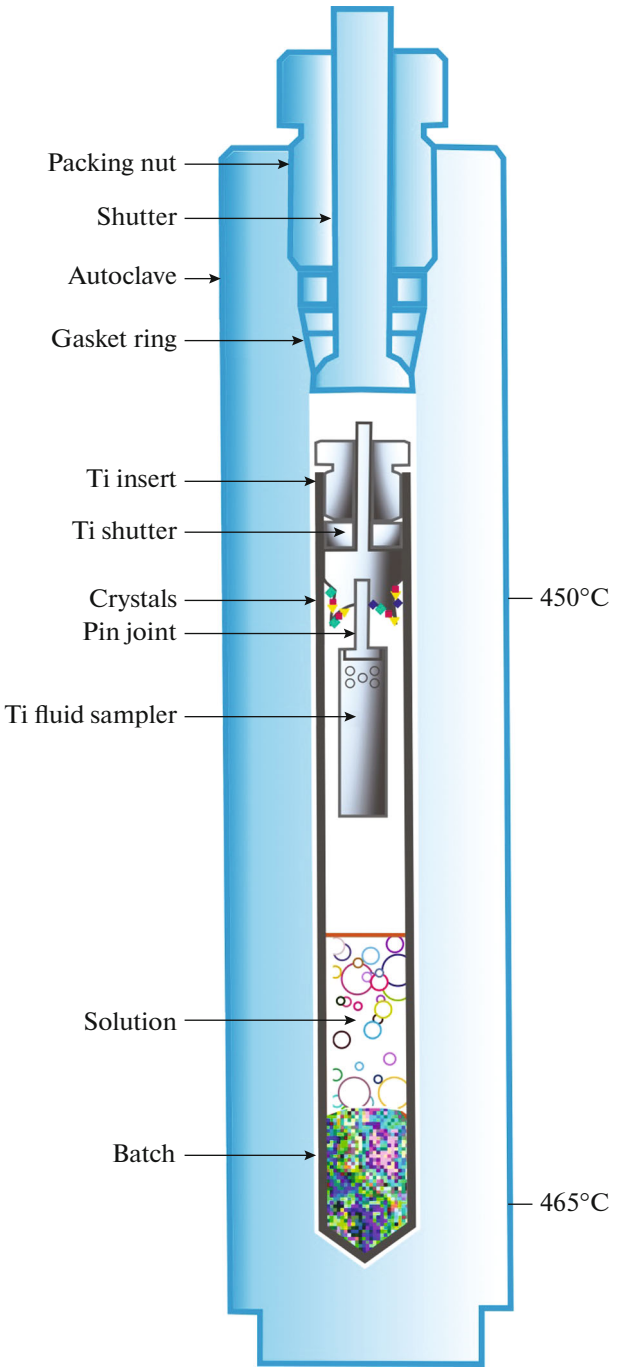

Fig. 1. Scheme of thermogradient hydrothermal synthesis.

quartz nebulizer chamber with cooling up to 3°C; sample introduction time of 60 s; spectra acquisition time 100–120 s, rinsing (3% HNO_3) time of 120–240 s, sensitivity of 10^6 imp/s per 1 ng/mL In, and the in-house Rh standard (2 ng/mL). The instrumental parameters were optimized using a tuning solution that contained 1 ppb of each analyzed element. Concentrations were calculated using certified SPEX CLMS-1-4 solutions (USA) with element concentrations of 0.1, 1.0, and 5.0 ng/mL and signal drift control

Table 1. Detection limits of elements in solutions (ICP-MS) and in crystals (LA-ICP-MS)

Element	In solution, ppm	In crystal, ppm
La	0.7	1.3
Ce	0.4	3.5
Pr	0.1	0.2
Nd	0.4	0.7
Sm	0.1	1.0
Eu	1.4	0.4
Gd	0.3	1.2
Tb	0.04	0.2
Dy	0.2	0.7
Ho	0.03	0.3
Er	0.1	0.4
Tm	0.02	n.a.
Yb	0.08	0.2
Lu	0.02	0.2

using the ^{103}Rh in-house standard. The matrix effect was eliminated by dilution of solutions of analyzed samples. The detection limits were estimated using 3σ criterion (Table 1). The results were controlled using standard multielement solutions (MERCK, Germany; NIST, USA).

The *Ln* contents in magnetite and hematite crystals were determined by LA-ICP-MS on an Agilent 7500ce (Agilent Tech., USA) using a New Wave Research UP-213 laser ablation system at the Limnological Institute of the Siberian Branch of the Russian Academy of Sciences. The experimental parameters were as follows: plasma power 1500 W, gas flow rates of 1.5 L/min, laser power 80%, frequency 10 Hz, beam size 55 μm, and acquisition time of 15 s. Scanning method was three spots per mass, with counting time of 0.1 s per one spot.

The calculations of *Ln* contents were based on the NIST 612 standard, which is suitable for obtaining reliable results when trace element concentrations in magnetite are of few ppm and lower (Nadoll et al., 2014; Smagunov et al., 2021). The calculated values of detection limits are presented in Table 1, and standard deviations, in Tables 2 and 3.

The results of LA-ICP-MS analysis in separate spots on crystal faces were processed using technique allowing the identification of evenly distributed component of *Ln* admixture formally corresponding to the structurally bound form (Tauson and Lustenberg, 2008). No stable results were obtained for Tm using this approach, and data on this element are constrained by its contents in solutions.

Ln-rich phases formed simultaneously with magnetite and hematite were studied by methods of Scanning Electron Microscopy using EDS Microanalysis System AztecLive Advanced Ultim Max 40 with nitrogen-free detector (Oxford Instruments Analytical Ltd., England) (SEM-EDS) and Electron Probe Microanalysis (EPMA) applying MIRA 3 LMH (TESCAN, Czech Republic) and Superprobe JXA 8200 (JEOL

Table 2. Lanthanide contents in magnetite (LA-ICP-MS), co-crystallization coefficients *Ln*/Fe and crystal/fluid partition coefficients

Element	$C_{Ln} \pm \Delta^*$, ppm		$D_{Ln/Fe}$		$D_{Ln}^{s/aq}$	
	Run 1	Run 2	Run 1	Run 2	Run 1	Run 2
La	3 ± 2	26 ± 5	4.1×10^{-3}	5.2×10^{-3}	0.9	1.4
Ce	2 ± 2	2.6 ± 0.4	5.7×10^{-3}	5.6×10^{-3}	1.3	1.6
Pr	12 ± 12	23 ± 5	1.1×10^{-2}	4.8×10^{-3}	2.5	1.4
Nd	13 ± 13	20 ± 5	1.0×10^{-2}	4.8×10^{-3}	2.3	1.3
Sm	6 ± 5	19 ± 5	6.0×10^{-3}	5.2×10^{-3}	1.4	1.5
Eu	5 ± 5	8 ± 2	2.2×10^{-3}	1.5×10^{-3}	0.5	0.4
Gd	10 ± 7	26 ± 7	7.9×10^{-3}	8.4×10^{-3}	1.8	2.4
Tb	12 ± 9	34 ± 9	1.0×10^{-2}	1.6×10^{-2}	2.2	4.4
Dy	16 ± 16	43 ± 10	1.4×10^{-2}	2.9×10^{-2}	3.2	3.9
Er	24 ± 24	52 ± 11	4.4×10^{-2}	7.3×10^{-2}	9.9	22.1
Tm	Not analyzed					
Yb	36 ± 32	50 ± 10	0.116	0.126	26.3	35.5
Lu	52 ± 48	58 ± 11	0.202	0.182	45.6	50.9

* Error was calculated for 0.90 significance level at spot number $n < 10$ and 0.95 at $n \geq 10$. Spot number for separate elements in final samplings was from 6 to11 (run1) and from 11 to 13 (run 2).

Table 3. Lanthanide contents in hematite (LA-ICP-MS), co-crystallization coefficients *Ln*/Fe and crystal/fluid partition coefficients

Element	$C_{Ln} \pm \Delta$*, ppm		$D_{Ln/Fe}$		$D_{Ln}^{s/aq}$	
	Run 3	Run 4	Run 3	Run 4	Run 3	Run 4
La	9 ± 6	28 ± 16	1.9×10^{-3}	3.5×10^{-3}	0.3	0.4
Ce	0.5 ± 0.2	4 ± 3	1.6×10^{-3}	7.4×10^{-2}	0.2	8.5
Pr	10 ± 6	32 ± 18	1.1×10^{-3}	8.5×10^{-3}	0.2	1.0
Nd	10 ± 6	30 ± 15	1.6×10^{-3}	1.0×10^{-2}	0.2	1.2
Sm	10 ± 5	23 ± 10	3.0×10^{-3}	1.3×10^{-2}	0.4	1.4
Eu	10 ± 4	21 ± 10	1.1×10^{-3}	5.1×10^{-3}	0.2	0.6
Gd	15 ± 4	25 ± 10	4.2×10^{-3}	1.5×10^{-2}	0.6	1.7
Tb	31 ± 10	35 ± 13	1.5×10^{-2}	3.6×10^{-2}	2.1	4.2
Dy	52 ± 14	50 ± 16	3.1×10^{-2}	7.0×10^{-2}	4.2	8.1
Er	112 ± 23	91 ± 30	0.119	0.254	16	29
Tm	Not analyzed					
Yb	328 ± 53	229 ± 46	0.609	0.94	84	107
Lu	571 ± 68	466 ± 155	1.322	2.192	182	250

* Error was calculated for significance level of 0.95. Spot number for separate elements in final samplings varies from 9 to 13 (run 3) and from 12 to 14 (run 4).

Ltd., Japan) devices at the Center for Collective Use "For Isotope and Geochemical Studies" in the Institute of Geochemistry, Siberian Branch of the Russian Academy of Sciences.

RESULTS AND DISCUSSION

During experiment, crystals of magnetite (hematite) mainly of octahedral (*Mt*) and rhombohedral (*Hem*) habit up to 1 mm in size (Fig. 2) were synthesized in the growth zone in association with lanthanide-rich phases represented by light yellow lamellar and dark red acicular crystals (Fig. 3).

Compositions of analyzed solutions (quenched from insert and collected in trap) are shown in Fig. 4.

The *Ln* contents measured by LA-ICP-MS and calculated partition and cocrystallization coefficients of *Ln* are presented in Tables 2 and 3 and in Fig. 5.

It is seen in Fig. 4 that lanthanides practically are not retained in solution after cooling (quenching). After cooling of system with hematite ($\log fO_2 > -21.6$ bar at 450°C), ~1.3–7.5% *Ln* are preserved (except for Ce and Eu, which preserve the high-temperature contents at 17 and 33%, respectively). In the system with magnetite (at lower fO_2), the *Ln* content in quenched solution is slightly higher (3.3–18% for most elements). Thereby, 33% Ce is preserved, while Eu is completely preserved. This suggests the higher stability of Ce and Eu complexes in the solution compared to other lanthanides. At the same time, the Eu co-crystallization coefficient does not increase and even shows obvious minimum (Fig. 5a), which is inconsistent with its inferred strong complexing in solution. According to (Migdisov et al., 2009), Eu chloride complexes at 150–250°C show no anomalies in the stability constants relative to the neighboring *Ln*. In the lanthanide series, these constants decrease only for heavy *Ln*—Tm, Yb, and Lu. However, judging from the formation of *Ln* oxychloride and oxyhydroxide (see below), the transfer in our experiments was provided by not only pure chloride complexes $LnCl^{2+}$ and $LnCl_2^+$,but also

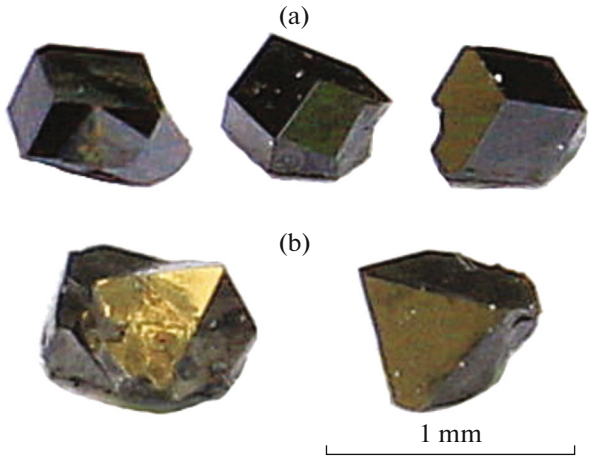

Fig. 2. Synthesized crystals of hematite (a) and magnetite (b): main habit forms.

Fig. 3. Own *Ln* phases in the hematite crystallization field (run 4). Lamellar crystals are hydrous oxychloride of mainly light and medium *Ln*, acicular crystals are oxyhydroxide of Fe and medium–heavy *Ln*, and equant rhombic crystals are hematite.

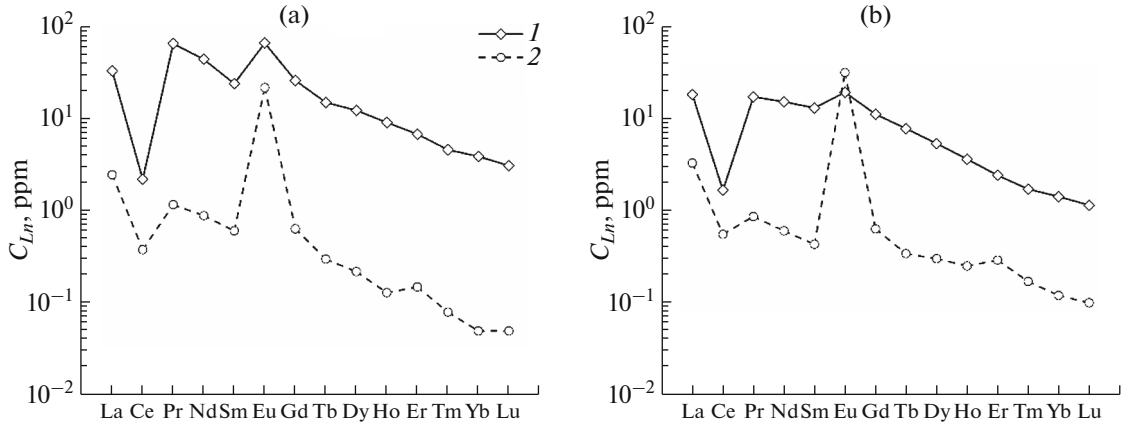

Fig. 4. The *Ln* contents in fluid from trap (*1*) and in quenched solution from insert (*2*) in runs on synthesis of hematite (a, run 3) and magnetite (b, run 2).

by hydroxychloride $Ln(OH)Cl^+$. Thus, the europium minimum in the fluid–mineral systems can be related not only with the absence of Eu mineral carriers, but also with its lower co-crystallization coefficient compared to other lanthanides (at least, for magnetite and hematite).

The $D_{Ce/Fe}$ maximum in hematite in run 4 can be explained by more oxidizing conditions at increasing addition of *Ln* oxides in batch. This suggests the possible appearance of significant amount of Ce^{4+} that is more strongly complexed in solution than Ce^{3+}. This is confirmed by the discovery of both these species on the hematite surface at similar conditions using X-ray photoelectron spectroscopy (Tauson et al., 2018). It should be however kept in mind that the Ce content in hematite in run 4 is close to the detection limit (Table 1) and even lower than detection limits in other cases.

Except for Eu, lanthanides are compatible in magnetite. Thereby, Er, Yb, and Lu are characterized by the relatively high degree of coherence (Table 2).

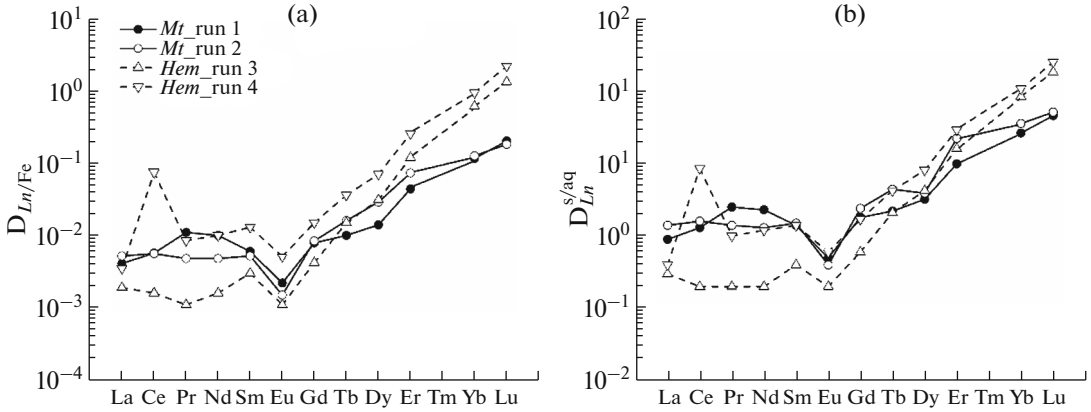

Fig. 5. Experimental results on the *Ln* distribution between magnetite (*Mt*), hematite (*Hem*), and hydrothermal solution at 450°C and pressure of 1 kbar. (a) *Ln*/Fe cocrystallization coefficient, (b) crystal–solution partition coefficient of *Ln*.

Experiments with hematite yield slightly different results, but tendency to the growth of coefficient with increasing atomic number *Ln* is preserved and even intensified compared to magnetite (Table 3). Heavy lanthanides, beginning from Tb, are compatible in hematite. The assignment of element to compatible (coherent) and incompatible (incoherent) is based on its partition coefficient between solid phase and solution: $D^{s/aq} > 1$ and $D^{s/aq} < 1$, respectively.

At present, it is difficult to determine whether the obtained estimates correspond to structurally bound admixture of Ln in minerals. Although LA-ICP-MS analysis was performed for crystals with smooth pure faces, the limited area of the latter due to small crystal size could cause partial capture of surface component, which is more abundant than structurally bound form (Smagunov et al., 2021). This is partially supported by the high dispersion of data in run 1 (Table 2), where magnetite crystals were smaller and the number of analyzed spots was likely insufficient. The EPMA and SEM-EDS analyses revealed no the presence of REE-rich phases in the magnetite and hematite crystals. While processing LA-ICP-MS data, we attempted to recognize the structurally bound REE component using technique proposed in (Tauson and Lustenberg, 2008). Unfortunately, due to a few number and small size of crystals, we failed to apply the technique allowing complete omitting of the surface component of REE admixture. For this reason, the obtained data are qualified as maximum estimates of "true" partition and co-crystallization coefficients for structurally bound *Ln* admixtures. Nevertheless, the application of obtained data for the determination of *Ln* proportions in hydrothermal solutions in any case is more justified than the use of low-temperature absorption partition constants K_d (e.g., Alibert, 2016). For hematite in NaCl solution, K_d for light and medium *Ln* are over three orders of magnitude higher than partition coefficients obtained by us, whereas K_d for heavy *Ln* (Yb, Lu) seem to be comparable with data in Table 3 (Tao et al., 2004). It should be reminded that the REE behavior at elevated temperatures differs from theoretical predictions, in particular, Pearson rules (Williams-Jones et al., 2012). In addition, this difference can be explained by different mechanisms of admixture uptake under normal or nearly normal conditions (adsorption) and in hydrothermal thermogradient systems, when the crystal growth is provided by the surface non-autonomous phase (Tauson et al., 2019).

Note especially a clear tendency to increase in co-crystallization coefficients for heavy *Ln*, beginning from Gd–Tb (Fig. 5). To some extent, this can be caused by the decrease of solubility of their oxides (spinels) of the corresponding stoichiometry and structural type relative to the solubility of ferruginous minerals (Chernyshev, 1980). Indeed, experimental results show that an increase of $D_{Ln/Fe}$ for heavy *Ln* is accompanied by the decrease of their contents relative to Fe in fluid and, to lesser extent, an increase of contents in the magnetite and hematite crystals. The latter can be explained by the effect of lanthanide compression: for instance, the Fe^{3+} substitution in the high-spin state in magnetite for Ln^{3+} in the octahedral site is controlled by the relative deviation of the effective ion radii by 37% for La and lower value (24%) for Lu.

The discovered effect could have important geochemical implication. It is believed that LREE have the higher geochemical mobility and are mainly transferred for greater distances from magma source compared to HREE (Williams-Jones et al., 2012). This would help to reveal the primary sources of ore elements. However, if fluid discharge will be accompanied by the formation of Fe oxide minerals, their subsequent analysis will show the HREE enrichment relative to LREE regardless of the distance to magmatic body due to the higher $D_{Ln/Fe}$ for HREE. Therefore, the application of this typochemical criterion (proportions of heavy and light *Ln*) for identification of REE source requires knowing their speciation and coeffi-

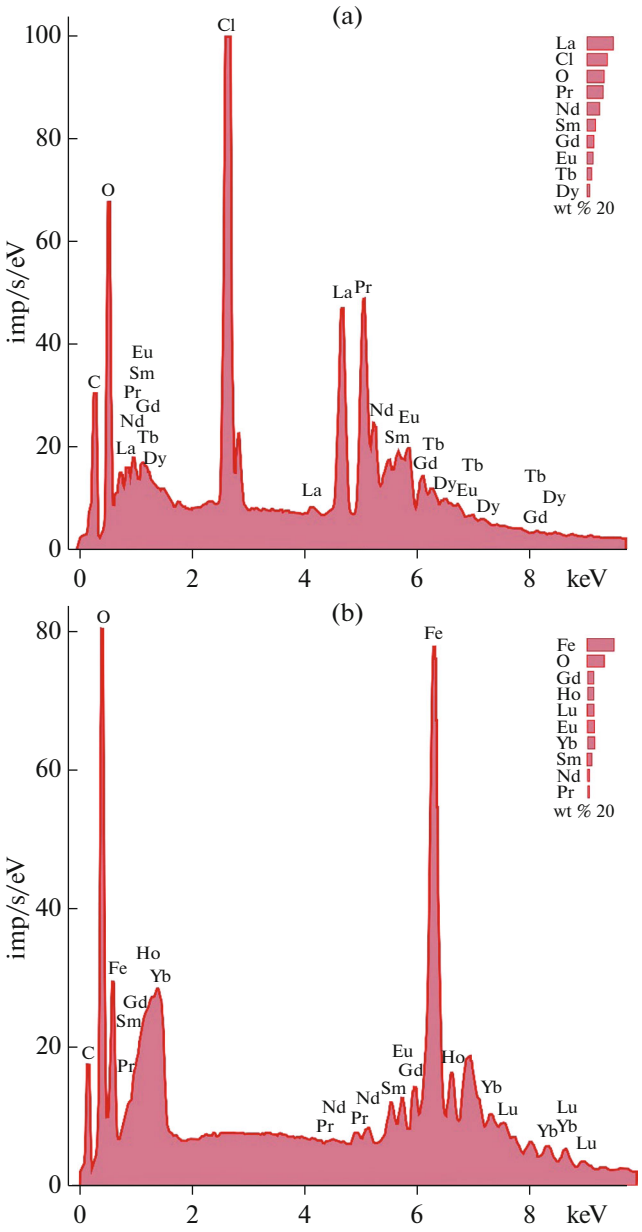

Fig. 6. Energy-dispersive X-ray spectrum (SEM-EDX) of lamellar (a) and acicular (b) crystals associated with magnetite and hematite (Fig. 2).

cients of co-crystallization in minerals—their potential carriers. The observations of own lanthanide minerals in ore occurrences could be helpful in this context.

In our experiments (both in the magnetite and hematite field), own *Ln* phases were synthesized simultaneously (as indicated by their intergrowths, Fig. 3) but have contrasting compositions. These phases have no analogues among known hydrothermal REE minerals mentioned in overview (Migdisov et al., 2016). At present, their study has not been completed yet, but according to preliminary data, yellow transparent crystals are aqueous *Ln* oxychloride, which can be represented by formula $LnClO{\bullet}H_2O$, where *Ln* are mainly light and medium lanthanides (La, Pr, Nd, Sm, Eu, Gd, and Tb) (Fig. 6a). Red acicular crystals are represented by Fe and *Ln* oxyhydroxide and, in contrast, are enriched in heavy *Ln*. Their idealized formula is $(Fe_{2/3}Ln_{1/3})OOH$, where *Ln* are represented by heavy and medium lanthanides (Lu, Yb, Ho, Tb, Gd, Eu, Sm, Nd) (Fig. 6b).

This example demonstrates that the coexistence of light and heavy REE within a single hydrothermal system is provided by the simultaneous crystallization of phases that selectively incorporate light and heavy lanthanides.

It is important for further experimental studies that an increase of Fe transfer in form of oxides in order to obtain larger crystals can be reached by eliminating the competitive Fe-bearing phase via transition to the more "acid" hydrothermal solution.

CONCLUSIONS

(1) The partition and co-crystallization coefficients of *Ln* in magnetite and hematite under hydrothermal conditions at 450°C and 1 kbar are determined, which are interpreted as maximum estimates of "true" coefficients for structurally bound admixtures.

(2) Since the majority of lanthanides are not retained in solution after quenching, the experiment on synthesis of iron oxide crystals should be accompanied by sampling of high-temperature fluid.

(3) Lanthanides (except for Eu) are compatible in hydrothermal magnetite. Thereby, Er, Yb, and Lu are characterized by the relatively high degree of coherence. Heavy *Ln*, beginning from Tb, are coherent elements in hematite.

(4) Tendency to increasing co-crystallization and partition coefficients for heavy *Ln*, beginning from Gd–Tb, is typical of both Fe oxides. This example shows that the application of such typochemical guide as proportions of heavy and light *Ln* for determining REE source requires knowing of their speciation and co-crystallization coefficients in minerals that are the potential REE carriers.

(5) Own *Ln* phases obtained in association with magnetite and hematite exemplifies the coexistence of light and heavy REE within a single hydrothermal system owing to the simultaneous crystallization of phases selectively incorporating light and heavy elements.

(6) An increase of acidity of mineralizing hydrothermal solution is likely required to provide the Fe transfer in favor of its oxides and, respectively, to obtain larger *Ln*-doped crystals.

ACKNOWLEDGMENTS

We are deeply grateful to N.N. Pakhomova and T.M. Pastushkova for help with analytical work. We thank scientific

editor A.Yu. Bychkov, as well as V.A. Alekseev, and anonymous reviewer for valuable comments and interest to our work.

FUNDING

This work was carried out in the framework of state assignment for the Vinogradov Institute of Geochemistry, project no. 0284-2021-0002. The studies were performed using facilities of the Center for Collective Use "For Isotope and Geochemical Studies" in the Institute of Geochemistry of the Siberian Branch of the Russian Academy of Sciences and "Ultramicroanalysis" in the Limnological Institute of the Siberian Branch of the Russian Academy of Sciences.

CONFLICT OF INTEREST

The authors declare that they have no conflicts of interest.

REFERENCES

C. Alibert, "Rare earth elements in Hamersley BIF minerals," Geochim. Cosmochim. Acta **184**, 311–328 (2016).

F. Chen, F. Liu, L. Wang, and J. Wang, "Comparison of the preparation process of rare earth oxides from the water leaching solution of waste Nd–Fe–B magnets' sulfate roasting products," Processes **10**, art. 2310 (2022).

L. V. Chernyshev, "On the theory of hydrothermal equilibria of minerals of variable composition," Geokhimiya, No. 6, 787–797 (1980).

D. E. Harlov, C. J. Meighan, I. D. Kerr, and I. M. Samson, "Mineralogy, chemistry, and fluid-aided evolution of the Pea Ridge Fe oxide-(Y plus REE) deposit, Southeast Missouri, USA," Econ. Geol. **111** (8), 1963–1984 (2016).

X. -W. Huang, M. -F. Zhou, Y. -Z. Qui, and L. Qi, "In-situ LA-ICP-MS trace elemental analyses of magnetite: The Bayan Obo Fe–REE–Nb deposit, North China," Ore Geol. Rev. **65**, 884–899 (2015).

N. A. Kulik and S. V. Melgunov, "On the evolution of mineral formation in complex hematite–fluorite–bastnaesite occurrences of South Tuva," Geol. Geofiz, No. 2, 93–103 (1992).

A. A. Migdisov, A. E. Williams-Jones, and T. Wagner, "An experimental study of the solubility and speciation of the rare earth elements (III) in fluoride- and chloride-bearing aqueous solutions at temperatures up to 300°C," Geochim. Cosmochim. Acta **73**, 7087–7109 (2009).

A. Migdisov, A. E. Williams-Jones, J. Brugger, and F. A. Caporuscio, "Hydrothermal transport, deposition, and fractionation of the REE: Experimental data and thermodynamic calculations," Chem. Geol. **439**, 13–42 (2016).

P. Nadoll, T. Angerer, J. L. Mauk, D. French, and J. Walshe, "The chemistry of hydrothermal magnetite: A review," Ore Geol. Rev. **61**, 1–32 (2014).

N. Smagunov, V. Tauson, S. Lipko, D. Babkin, T. Pastushkova, O. Belozerova, and N. Bryansky, "Partitioning and surficial segregation of trace elements in iron oxides in hydrothermal fluid systems," Minerals **11** (1), art. 57 (2021).

F. H. B. Tallarico, B. R. Figueiredo, D. I. Groves, N. Kositcin, N. J. McNaughton, I. R. Fletcher, and J. L Rego, "Geology and SHRIMP U-Pb geochronology of the Igarape Bahia deposit, Carajas Copper-Gold belt, Brazil: An Archean (2.57 Ga) example of iron-oxide Cu–Au(U–REE) mineralization," Econ. Geol. **100** (1), 7–28 (2005).

Z. Tao, X. Wang, Z. Guo, and T. Chu, "Is there a tetrad effect in the adsorption of lanthanides (III) at solid-water interfaces?," Colloids and Surfaces A: Phys. Eng. Aspects. **251**, 19–25 (2004). Doi: https://doi.org/10.1016/j.colsurfa.2004.08.078

V. L. Tauson and E. E. Lustenberg, "Quantitative determination of modes of gold occurrence in minerals by the statistical analysis of analytical data samplings. Geochem. Int. **46** (4), 423–428 (2008).

V. L. Tauson, S. V. Lipko, N. V. Smagunov, and R. G. Kravtsova, "Trace element partitioning dualism under mineral–fluid interaction: Origin and geochemical significance," Minerals **8**, art. 282 (2018).

V. L. Tauson, S. V. Lipko, K. Yu. Arsent'ev, and N. V. Smagunov, "Crystal growth through the medium of nonautonomous phase: implications for element partitioning in ore systems," Cryst. Rept. **64** (3), 496–507 (2019).

A. E. Williams-Jones, A. A. Migdisov, and I. M. Samson, "Hydrothermal mobilization of the rare earth elements – a tale of "Ceria" and "Yttria," Elements **8**, 355–360 (2012).

H. Zamanian and K. Radmard, "Geochemistry of rare earth elements in the Baba Ali magnetite skarn deposit, western Iran – a key to determine conditions of mineralization," Geologos **22** (1), 33–47 (2016).

Translated by M. Bogina